

Two Remarkable Spherical Arrangements of Circles

Hellmuth Stachel

Vienna University of Technology, 1040 Vienna, Austria,
stachel@dmg.tuwien.ac.at,
WWW home page: <http://www.dmg.tuwien.ac.at/stachel>

Abstract. Inspired by recent publications of K. Myriantis and of A.W. Akopyan and A.I. Bobenko, two different arrangements of circles on the sphere are studied. The first one originates from Phyllotaxis, a topic in plant morphogenesis, and gives rise to a polyhedron with hexagonal faces and a covering of the sphere with circles in a spiral arrangement. The second is related to a Poncelet grid on the sphere. The extended n sides of a closed spherical billiard within a conic form a net with a finite number of quadrilaterals with incircles. Orthogonality transforms it into a configuration of n concurrent lines where each pair is ‘concurrent’ with $n-2$ other pairs, i.e., the four lines are inscribed into a cone of revolution.

Keywords: spiral grid, hyperbolic screw motion, incircular net, Ivory’s Theorem

1 Introduction

Alfred Clebsch described Plücker’s method of research as drawn particularly from “*die Freude an der Gestalt*”, to say, driven by an appreciation for aesthetics and intuition [10]. The same can be said about this research.

The presented arrangements of circles on the sphere (see Figs. 3, right, and 6) are closely related to two recent publications. The first has been written by K. Myriantis [11], the second by A.W. Akopyan and A.I. Bobenko [1]. We recall both results and show a few consequences.

2 A polyhedron with hexagonal faces and a circumsphere

In the Euclidean plane, let σ_1, σ_2 be two different stretch-rotations with the common center O , i.e., the commutative products of rotations about O through the respective signed angles α_1, α_2 and dilations with center O and dilation factors $\delta_1, \delta_2 \neq 1$. Then the orbit of any point $P \neq O$, i.e., the set of points $P_{ij} = \sigma_1^i \sigma_2^j(P)$ for $i, j \in \mathbb{Z}$, is called a *spiral grid* (Fig. 1). The spiral grid does not change when a basic transformation σ_i is replaced by its inverse. Hence, it means no restriction to require that both dilatation factors δ_1, δ_2 are smaller than 1.

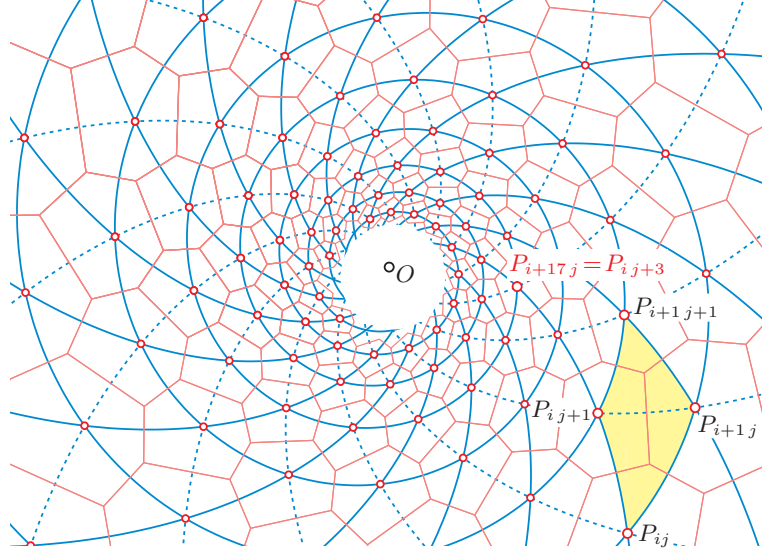


Fig. 1. Closed spiral grid, its Delaunay triangulation with edges along logarithmic spirals, and its Voronoi cells.

The spiral grid is called *closed* ([11, p. 180]) if there are $n_1, n_2 \in \mathbb{N}$ such that $\sigma_1^{n_1} = \sigma_2^{n_2} \circ \rho_{2\pi}$, where $\rho_{2\pi}$ denotes the rotation about O through 2π . In this case we have $P_{i+n_1j} = P_{ij+n_2}$ for all $i, j \in \mathbb{Z}$. Figure 1 shows an example with $\alpha_1 = 23.5^\circ$, $\delta_1 = 0.942$, $\alpha_2 = 13.167^\circ$, $\delta_2 = 0.71278$, and $(n_1, n_2) = (17, 3)$ (note point $P_{i+17j} = P_{ij+3}$).

A closed spiral grid¹ can also be defined as the set of points of intersection between logarithmic spirals. If the initial point $P = P_{00}$ has the polar coordinates $(r_0, 0)$ then these spirals arise from one of the curves with polar equations

$$r = r_0 e^{b_i \varphi} \quad \text{with} \quad b_i = \frac{1}{\alpha_i} \ln \delta_i \quad \text{for} \quad i = 1, 2 \quad (1)$$

by rotations about O through multiples of angles $\frac{2\pi}{n_2}$ and $\frac{2\pi}{n_1}$, respectively.

Stretch-rotations with a common center form a commutative group. Therefore the spiral grid of any point P remains unchanged if we replace the two basic transformations σ_1, σ_2 by

$$\sigma'_1 = \sigma_1^{c_1} \circ \sigma_2^{c_2} \quad \text{and} \quad \sigma'_2 = \sigma_1^{d_1} \circ \sigma_2^{d_2}, \quad \text{where} \quad c_1, c_2, d_1, d_2 \in \mathbb{Z} \quad \text{and} \quad c_1 d_2 - c_2 d_1 = 1.$$

σ'_1 takes the initial point P of the spiral grid to $P_{c_1 c_2}$. Similarly, σ'_2 sends P to $P_{d_1 d_2}$. The original stretch-rotations can be expressed in terms of σ'_1, σ'_2 as

$$\sigma_1 = (\sigma'_1)^{d_2} \circ (\sigma'_2)^{-c_2} \quad \text{and} \quad \sigma_2 = (\sigma'_1)^{-d_1} \circ (\sigma'_2)^{c_1}.$$

¹ For applications in *Phyllotaxis*, a topic of plant morphogenesis, see, e.g., [9] or [14].

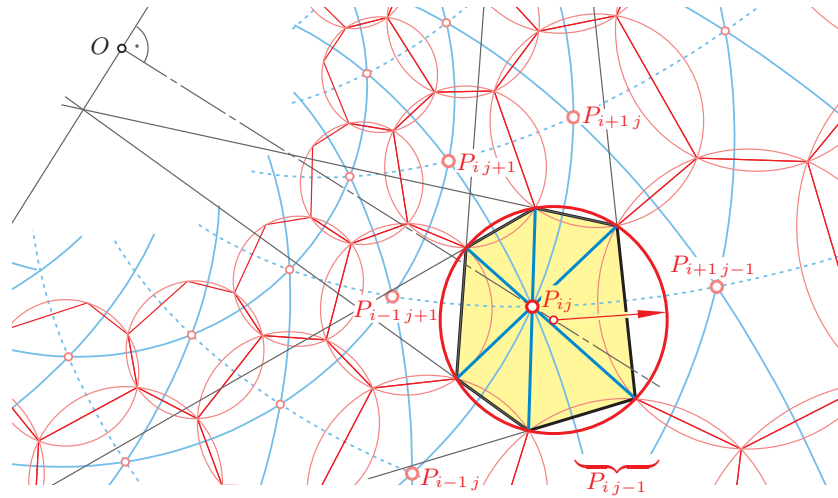


Fig. 2. Voronoi cells are concircular hexagons with concurrent main diagonals.

Obviously, $\gcd(c_1, c_2) = \gcd(d_1, d_2) = 1$, i.e., these pairs of integers must be relatively prime.

We confine ourselves to the general case, where the Delaunay triangulation of the grid is unique, which means that no two adjacent triangles share the circumcircle. Then the Voronoi cells² are hexagonal. In the excluded case the Voronoi cells are concircular quadrangles (note [11, Figs. 3–5]).

Of course, the net of Voronoi cells and its dual graph, the Delaunay triangulation, are invariant against the stretch-rotations σ_1, σ_2 . Without restriction of generality we may assume that the basic transformations are chosen such that $P_{ij}P_{i+1j}P_{ij+1}$ and $P_{i+1j}P_{ij+1}P_{i+1j+1}$ are two adjacent triangles of the Delaunay triangulation so that the logarithmic spirals corresponding to σ_1, σ_2 and $\sigma_1^{-1} \circ \sigma_2$ contain edges of the Delaunay graph (Fig. 1).

Myrianthis proved in [11, Theorem 2] that in the general case the mutually similar Voronoi cells are convex hexagons with concurrent main diagonals and a circumcircle (see Fig. 2). The proof is based on two properties: (i) opposite sides of the hexagons include the respective angles α_1, α_2 and $\alpha_2 - \alpha_1$; (ii) vertices of the hexagons form isosceles triangles with two adjacent grid points.

Now we apply a stereographic projection from the plane onto a sphere \mathcal{S} , e.g., with the South Pole as center and the North Pole as the image of O . Then (note Fig. 3) the images of the infinitely many circumcircles cover \mathcal{S} such that each circle is intersected by six neighboring circles, while each point of intersection is the meet of three circles. At every second point of intersection the respective angles between the circles are congruent because of the conformity of the stereographic projection.

² The Voronoi cell of point P_{ij} is the set of points X for which no other grid point is closer than P_{ij} .

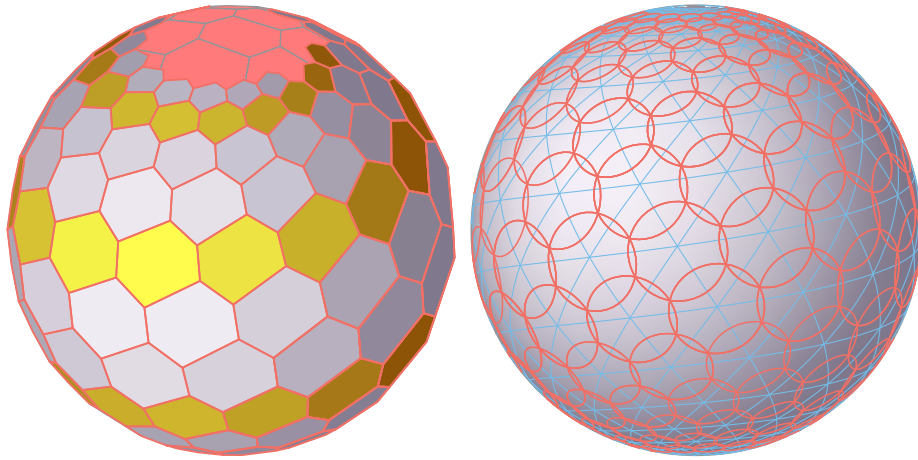


Fig. 3. Voronoi cells and circumcircles stereographically projected.

The existence of a circumcircle guarantees that for each Voronoi cell the images of the six vertices are coplanar. These hexagons form a polyhedron with

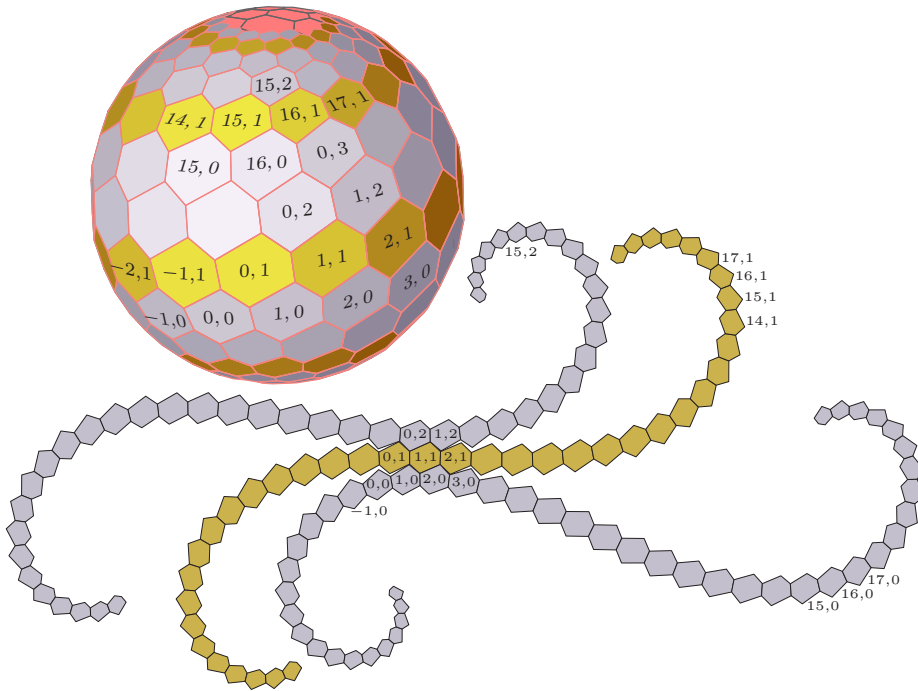


Fig. 4. Polyhedron and its development, scaled down to 40%.

infinitely many faces in a spiral pattern. The images of the logarithmic spirals are loxodromes on \mathcal{S} (Fig. 3, right).

Figure 4 shows the development of a part of the polyhedron, in size scaled to 40%. The spiral-like sequences of hexagons on \mathcal{S} , like the one colored in gold, yield in the development bands of S-shape. This is in accordance with Wunderlich's result [13] on peeling an apple and caused by the fact, that the sign of the geodesic curvature of spherical loxodromes changes when they cross the equator.

After applying affine or collinear transformations on the spherical polyhedron, we obtain polyhedra with hexagonal faces inscribed in ellipsoids, one-sheet hyperboloids or elliptic paraboloids, thus giving rise to piecewise linear approximations of these quadrics.

The faces of the spherical polyhedron (Fig. 3, left) are mutually incongruent, from the Euclidean point of view. However, it makes sense to interpret this polyhedron in the projective model of hyperbolic geometry, taking into account that the stereographic projection onto \mathcal{S} transforms the group of Möbius transformations in the plane onto hyperbolic motions, when \mathcal{S} serves as absolute quadric. A detailed analysis reveals that the stretch-rotation σ_i is transformed onto a hyperbolic screw motion with α_i as angle of rotation and $\ln \delta_i$ as hyperbolic length of translation along the axis a , which in our particular case connects the two poles. This motion preserves each surface \mathcal{Z} of constant distance to the axis a . In our model these hyperbolic 'cylinders' \mathcal{Z} , also called *Clifford surfaces*, are Euclidean ellipsoids of revolution. An affine transformation mapping \mathcal{S} onto one of these ellipsoids, while a remains pointwise fixed, can also be used to transform our polyhedron onto a polyhedron inscribed in \mathcal{Z} .

Theorem 1 *If the sphere \mathcal{S} is the absolute surface of the Cayley-Klein model of three-dimensional hyperbolic geometry then any two hexagons of the spiral polyhedron inscribed in \mathcal{S} arise from each other by hyperbolic screw motions about a common axis a . The loxodromes are hyperbolic screws. The same holds for affine images inscribed in a Clifford surface \mathcal{Z} .*

Remark. Due to Theorem 1, the polyhedron inscribed into the Clifford surface, can be generated by helical motions about the axis a . However, the Euclidean circumcircles of the hexagons are no more circles in the hyperbolic sense but mutually congruent planar sections of the Clifford surface.

3 An incircular net on the sphere

Recently I. Izmetiev and S.S. Tabachnikov in [8] and A.W. Akopyan and A.I. Bobenko in [1] revisited the following theorem (see Fig. 5).

Theorem 2 *If the tangents drawn from any two points A_1, B_1 of a conic c_1 to a confocal conic c_0 form a quadrilateral then each other pair of opposite vertices (A_i, B_i) , $i = 2, 3$, belongs to the same conic c_i of the confocal family. The quadrilateral is 'incircular', i.e., it has an incircle.*

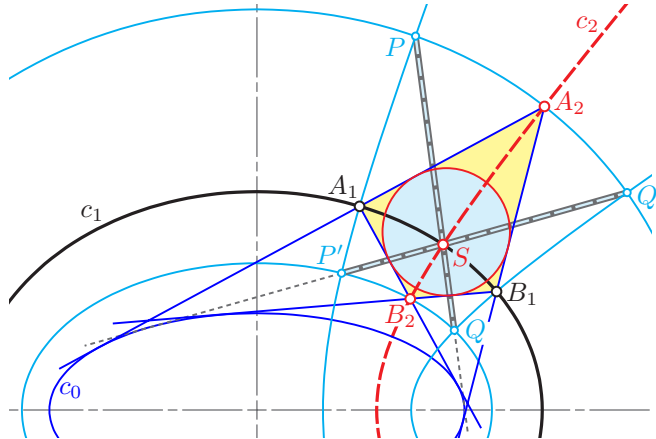


Fig. 5. An incircular quadrangle of tangents $A_1A_2B_1B_2$ (Theorem 2).

This theorem, which holds in non-Euclidean geometries as well, has already been published by Chasles [6, p. 841] and later by Böhm in [4, p. 221]. A projective version of this statement is given in [12] and proved using Chasles's ideas. The proof reveals that the theorem is valid also in the limiting case where two tangents coincide, i.e., the connecting line A_1B_1 contacts c_0 at the point B_2 . Then also the incircle contacts c_0 at B_2 (note Fig. 6).

The second part of Theorem 2, which is also discussed in [5], can be concluded from Ivory's Theorem, as shown in Fig. 5: The respectively second confocal conics through A_1 , B_1 , A_2 , and B_2 define a curvilinear quadrangle $PP'QQ'$ with diagonals of equal lengths $\overline{PQ} = \overline{P'Q'}$, by virtue of Ivory's Theorem. The conics c_1 and c_2 divide this quadrangle into four subtriangles. Due to a general statement, the diagonal lines in each Ivory quadrangle are tangents of the same confocal conic c_0 (see, e.g., [2, p. 118] or [3, p. 153]). Hence, pairs of diagonals passing through S must be aligned; S is the crossing point of PQ and $P'Q'$. Now, due to Ivory's Theorem, we can immediately figure out that in the quadrangle $A_1A_2B_1B_2$ the sums of lengths of opposite sides equals \overline{PQ} .

As already mentioned in [5], this incircular quadrangle can be extended to an *incircular net*, based on Poncelet grids (see, e.g., [7, p. 412]). While in [1] the Euclidean and hyperbolic cases are emphasized, we focus here on the spherical model of elliptic geometry. This has the advantage that only a finite number of circles is involved.

For designing a spherical Poncelet grid, we start with a closed billiard in the conic c_1 with $n > 4$ edges tangent to c_0 ; Figure 6 shows the cases $n = 13$ and $n = 9$. The extended sides of the billiard form a grid of n great circles which, in general, admits no symmetry. Any two pairs of adjacent great circles form two antipodal spherical quadrangles with incircles. This gives rise to the depicted *incircular net* [1, 5]. If the great circles are numbered in their natural order by $1, \dots, n$ then the points of intersection between the circles i and $i + k \pmod{n}$

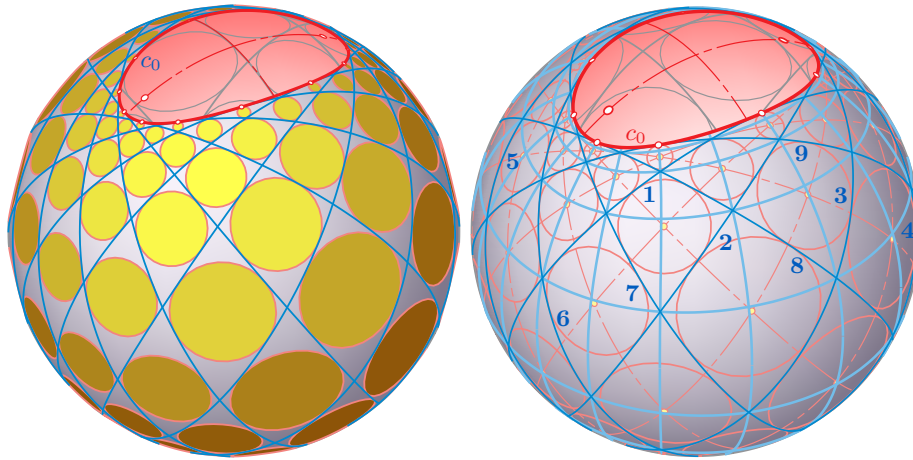


Fig. 6. Spherical incircular nets of $n = 13$ (left) and $n = 9$ (right) great circles. The right figure shows also the corresponding Poncelet grid.

for $i = 1, \dots, n$ and constant $k \in \mathbb{N}$ belong to another conic c_k confocal with c_0 and c_1 . Similarly, the great circles with labels i and $k - i \pmod n$ intersect on conics \bar{c}_k . The conics $c_0, \dots, c_{n-1}, \bar{c}_0, \dots, \bar{c}_{n-1}$ form a Poncelet grid (Fig. 6, right).

Due to Theorem 2, also the great circles $i, i+k, i+j, i+j+k$ (indices modulo n) define a pair of antipodal incircles, provided that either the four indices are mutually different, or at most two of them are equal. Figure 7 shows on the left hand side all possible circles for $n = 7$.

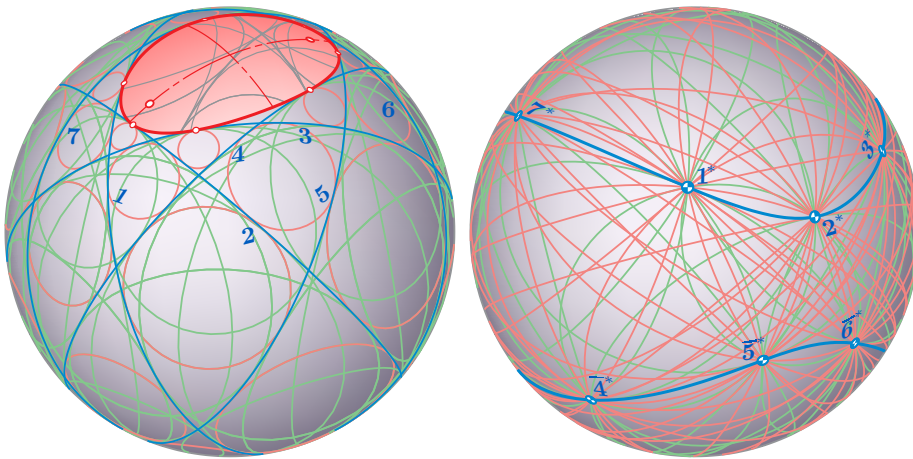


Fig. 7. Left: all 42 pairs of antipodal incircles for $n = 7$. Right: dual version: all quadruples of admissible points out of $\{1^*, \dots, 7^*\}$ have a circumcircle.

After applying the elliptic absolute polarity, which in the line bundle model is equivalent to Euclidean orthogonality, we get other arrangements. The n great circles are converted into lines d_1, \dots, d_n on a quadratic cone. Note that, in general, these lines admit no symmetry. Four lines $d_i, d_j, d_{i+k}, d_{j+k}$ with indices modulo n are always elliptic-concircular, i.e., they are located on a cone of revolution.

In the sphere model we obtain pairs (i^*, \bar{i}^*) of antipodal points, which for $i = 1, \dots, n$ are placed on a pair of antipodal spherical conics. When polarizing incircles c , we have to take into account that, depending on the side of the great circle i , where the touching small circle c is located, the absolute polar circle c^* passes through one of the spherical centers i^* of i or its antipode \bar{i}^* . Each c^* passes through four points taken from the set $\{1^*, \bar{1}^*, 2^*, \dots, \bar{n}^*\}$ of $2n$ points. Hence, these quadruples of points must be coplanar. In Fig. 7, right, all visible circles through coplanar point quadruples are displayed.

References

1. Akopyan, A.V., Bobenko, A.I.: Incircular nets and confocal conics. Trans. Amer. Math. Soc. (2017) arXiv:1602.04637v2[math.DS]27Oct2017
2. Baker, H.F.: Principles of Geometry, vol. III, Solid Geometry. Cambridge at the University Press (1923)
3. Böhm, W.: Die Fadenkonstruktionen der Flächen zweiter Ordnung. Math. Nachr. 13, 151–156 (1955)
4. Böhm, W.: Ein Analogon zum Satz von Ivory. Ann. Mat. Pura Appl. (4) 54, 221–225 (1961)
5. Böhm, W.: Verwandte Sätze über Kreisvierseitnetze. Arch. Math. 21, 326–330 (1970)
6. Chasles, M.: Propriétés générales des arcs d'une section conique, dont la différence est rectifiable. Comptes Rendus hebdomadaires de séances de l'Académie des sciences 17, 838–844 (1843)
7. Glaeser, G., Stachel, H., Odehnal, B.: *The Universe of Conics*. Springer Spectrum, Berlin Heidelberg (2016)
8. Izmistiev, I., Tabachnikov, S.: Ivory's Theorem revisited. Journal of Integrable Systems 2/1, xyx006 (2017), (<https://doi.org/10.1093/integr/xyx006>)
9. Jean, R.V.: Phyllotaxis, a systemic study in plant morphogenesis. Cambridge University Press, (1994)
10. Lorenat, J.: Die Freude an der Gestalt: Methods, Figures, and Practices in Early Nineteenth Century Geometry. PhD Thesis, Simon Fraser University (Canada); Université Pierre et Marie Curie (Paris 6) (2015)
11. Myriantthis, K.: Geometry and Design of Hexagonal Spirals (Voronoi and other). J. Geom. Graphics 21/2, 179–192 (2017)
12. Stachel, H.: Recalling Ivory's Theorem. Proceedings Mongeometrija 2018, Novi Sad/Serbia (in print)
13. Wunderlich, W.: Geometrische Betrachtungen um eine Apfelschale. Elem. Math. 15, 60–66 (1960)
14. Yamagishi, Y., Sushida, T., Hizume, A.: Voronoi Spiral Tilings. Nonlinearity 28/4, 1077–1102 (2015)